iScience

CellPress
OPEN ACCESS

Article

LncRNA SNHG5 adversely governs follicular growth in PCOS via miR-92a-3p/CDKN1C axis

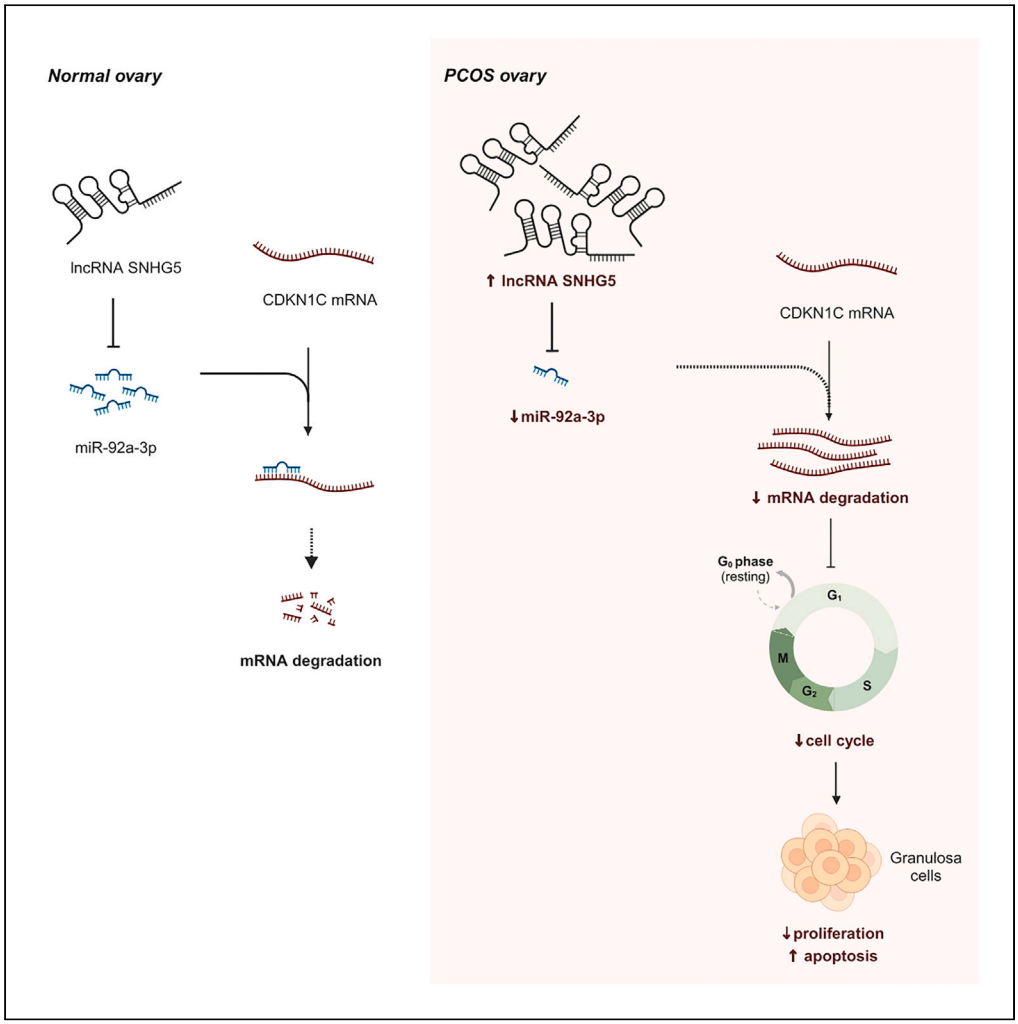

Zuwei Yang, Jiexue Pan, Chengliang Zhou, ..., Jianzhong Sheng, Li Jin, Hefeng Huang

jinli96@163.com (L.J.)
huanghefg@hotmail.com (H.H.)

Highlights

SNHG5 is upregulated in granulosa cells (GCs) of PCOS women

Overexpression of SNHG5 can induce PCOS-like features in mice

SNHG5 inhibits GC proliferation, induces apoptosis, and causes cell-cycle arrest

SNHG5 may exert its function through the miR-92a-3p/CDKN1C axis

Yang et al., iScience *27*, 108522
February 16, 2024
https://doi.org/10.1016/j.isci.2023.108522

iScience

CellPress
OPEN ACCESS

Article

LncRNA SNHG5 adversely governs follicular growth in PCOS via miR-92a-3p/CDKN1C axis

Zuwei Yang,[1,2,3,6] Jiexue Pan,[1,3,6] Chengliang Zhou,[2,6] Chuanjin Yu,[1] Zhiyang Zhou,[1] Guolian Ding,[1] Xinmei Liu,[1] Jianzhong Sheng,[1] Li Jin,[1,3,*] and Hefeng Huang[1,2,3,4,5,7,*]

SUMMARY

Small nucleolar RNA host genes (SNHGs) have been implicated in various biological processes, yet their involvement in polycystic ovary syndrome (PCOS) remains elusive. Specifically, SNHG5, a long non-coding RNA implicated in several human cancers, shows elevated expression in granulosa cells (GCs) of PCOS women and induces PCOS-like features when overexpressed in mice. *In vitro*, SNHG5 inhibits GC proliferation and induces apoptosis and cell-cycle arrest at G0/G1 phase, with RNA-seq indicating its impact on DNA replication and repair pathways. Mechanistically, SNHG5 acts as a competing endogenous RNA by binding to miR-92a-3p, leading to increased expression of target gene *CDKN1C*, which further suppresses GC proliferation and promotes apoptosis. These findings elucidate the crucial role of SNHG5 in the pathogenesis of PCOS and suggest a potential therapeutic target for this condition. Additional investigations such as large-scale clinical studies and functional assays are warranted to validate and expand upon these findings.

INTRODUCTION

Polycystic ovary syndrome (PCOS) is the most common endocrine and metabolic disorder in women of reproductive age, with a prevalence ranging from 6% to 20%.[1] According to the Rotterdam criteria,[2] the diagnosis of PCOS is based on the presence of at least two of the following characteristics: clinical and/or biochemical hyperandrogenism, ovulatory dysfunction, and polycystic ovarian morphology, which excludes other specific diagnoses. Heterogeneous by nature, the exact etiology and pathophysiology of PCOS remain largely obscure.[3] However, abnormalities of folliculogenesis have been well documented in anovulatory women with PCOS, including an accumulation of growing preantral follicles and arrest of follicle development beyond mid-antral stage.[4–6] Despite significant research, the mechanisms underlying aberrant follicle development in PCOS require further investigation. Granulosa cells (GCs) play a critical role in follicle development and ovulation by providing essential nutrients and a supportive microenvironment around the oocyte.[7] It has been reported follicular growth is regulated by survival and death of GCs[8–10] and that proper follicle development is dependent on an adequate number of GCs.[11] Abnormal proliferation and apoptosis of GCs may contribute to the pathogenesis of aberrant follicle development observed in PCOS women.[12–14]

Long non-coding RNAs (lncRNAs) are a class of transcripts greater than 200 nucleotides in length that do not commonly encode proteins.[15] Some investigations have emphasized their potential involvement in PCOS.[16] In our previous RNA-sequencing (RNA-seq) analysis, we found a significant increase of small nucleolar RNA (snoRNA) host gene 5 (SNHG5) expressions in GCs from PCOS women.[17] SNHG5 belongs to the SNHG family, which comprises a group of lncRNA.[18] SNHGs were previously reported to mainly act as carriers of snoRNAs.[18] However, recent studies have reported their involvement in various cellular processes such as cell proliferation, apoptosis, progression, metastasis, and chemoresistance in different cancers,[19,20] thus attracting increasing attention. In this study, we profiled the expression of 19 SNHGs in GCs of PCOS women, and found 12 of these SNHGs were significantly elevated in PCOS women compared to controls. Among the 12 SNHGs, SNHG5 was the most highly upregulated. SNHG5, also known as U50HG, is located on chromosome 6q14.3 and consists of six exons and five introns.[21] The exons splice into lncRNA SNHG5, while introns 4 and 5 encode snoRNA U50 and U50′, correspondingly.[21] SNHG5 has been implicated in various cancers,[21] but its role in PCOS

[1]Obstetrics and Gynecology Hospital, Institute of Reproduction and Development, Fudan University, Shanghai, China
[2]The International Peace Maternity and Child Health Hospital, School of Medicine, Shanghai Jiao Tong University, Shanghai, China
[3]Research Units of Embryo Original Diseases, Chinese Academy of Medical Sciences (No. 2019RU056), Shanghai, China
[4]Shanghai Key Laboratory of Reproduction and Development, Shanghai, China
[5]Key Laboratory of Reproductive Genetics (Ministry of Education), Department of Reproductive Endocrinology, Women's Hospital, Zhejiang University School of Medicine, Hangzhou, China
[6]These authors contributed equally
[7]Lead contact
*Correspondence: jinli96@163.com (L.J.), huanghefg@hotmail.com (H.H.)
https://doi.org/10.1016/j.isci.2023.108522

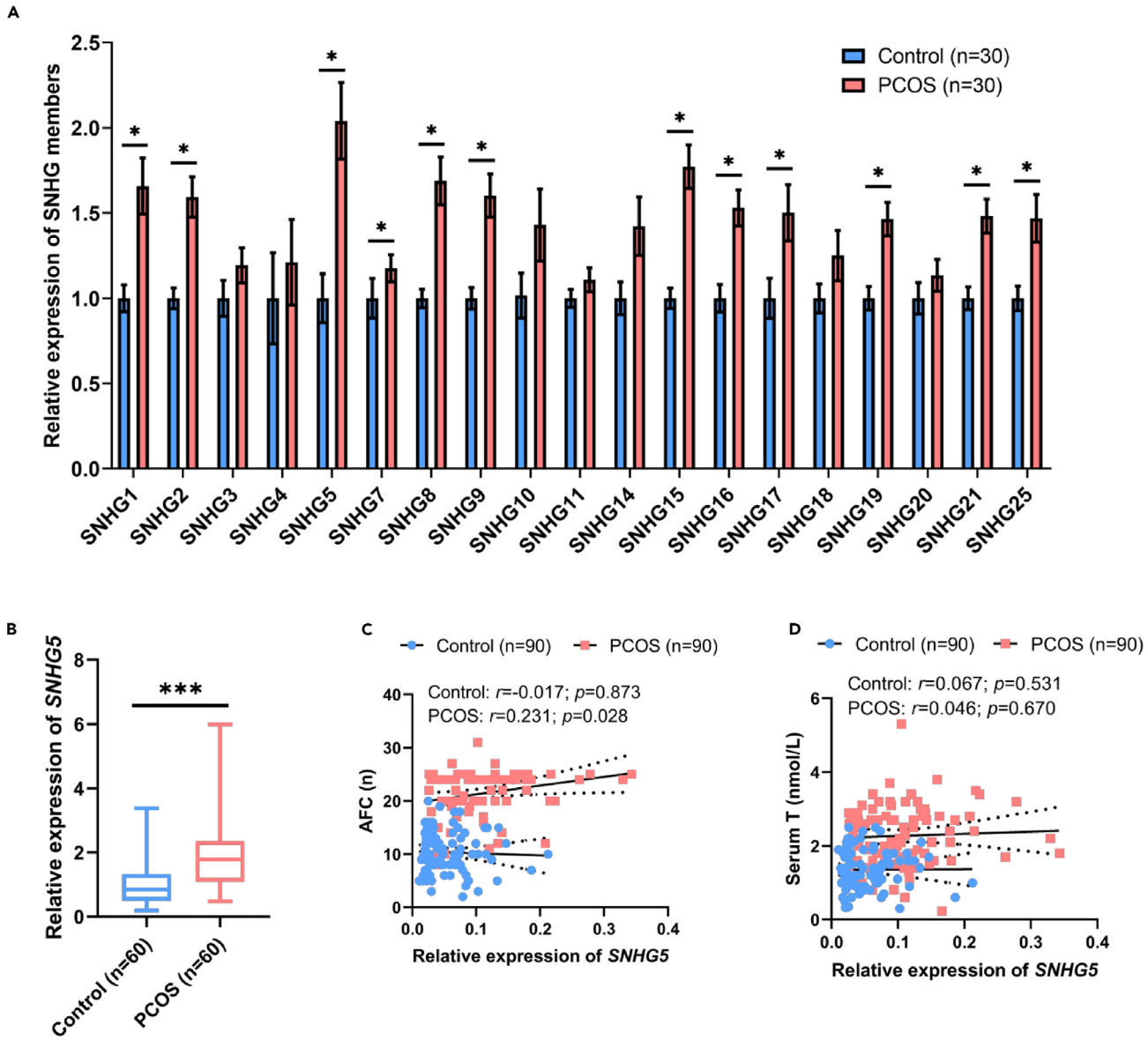

Figure 1. LncRNA SNHG5 is upregulated in granulosa cells from PCOS women

(A) Relative expression of SNHG family members in granulosa cells from 30 controls and 30 PCOS women (Cohort 1) analyzed by qRT-PCR.

(B) Relative expression of SNHG5 in granulosa cells from an independent cohort (Cohort 2) consisting of 60 controls and 60 PCOS patients.

(C) Correlation between SNHG5 expression levels in granulosa cells and antral follicle count (AFC) in a combined cohort of 90 PCOS women and 90 controls (Cohort 1 + Cohort 2).

(D) Correlation between SNHG5 expression levels in granulosa cells and serum testosterone (T) levels in a combined cohort of 90 women with PCOS and 90 controls (Cohort 1 + Cohort 2).

Data in (A) are presented as mean ± SEM, while (B) is represented as a box-whisker plot. Statistical significance in (A) and (B) was determined by Mann-Whitney U test. *p < 0.05; **p < 0.01; ***p < 0.001.

remains unclear. Therefore, we explored the expression, clinical significance, function and underlying mechanisms of SNHG5 in PCOS in this study.

RESULTS

LncRNA SNHG5 is upregulated in granulosa cells from women with PCOS

To identify differentially expressed SNHGs, we analyzed a panel of 19 SNHGs in GCs from 30 PCOS women and 30 controls (cohort 1) by quantitative reverse transcription-polymerase chain reaction (RT-qPCR). Among the SNHGs quantified, we found the upregulation of

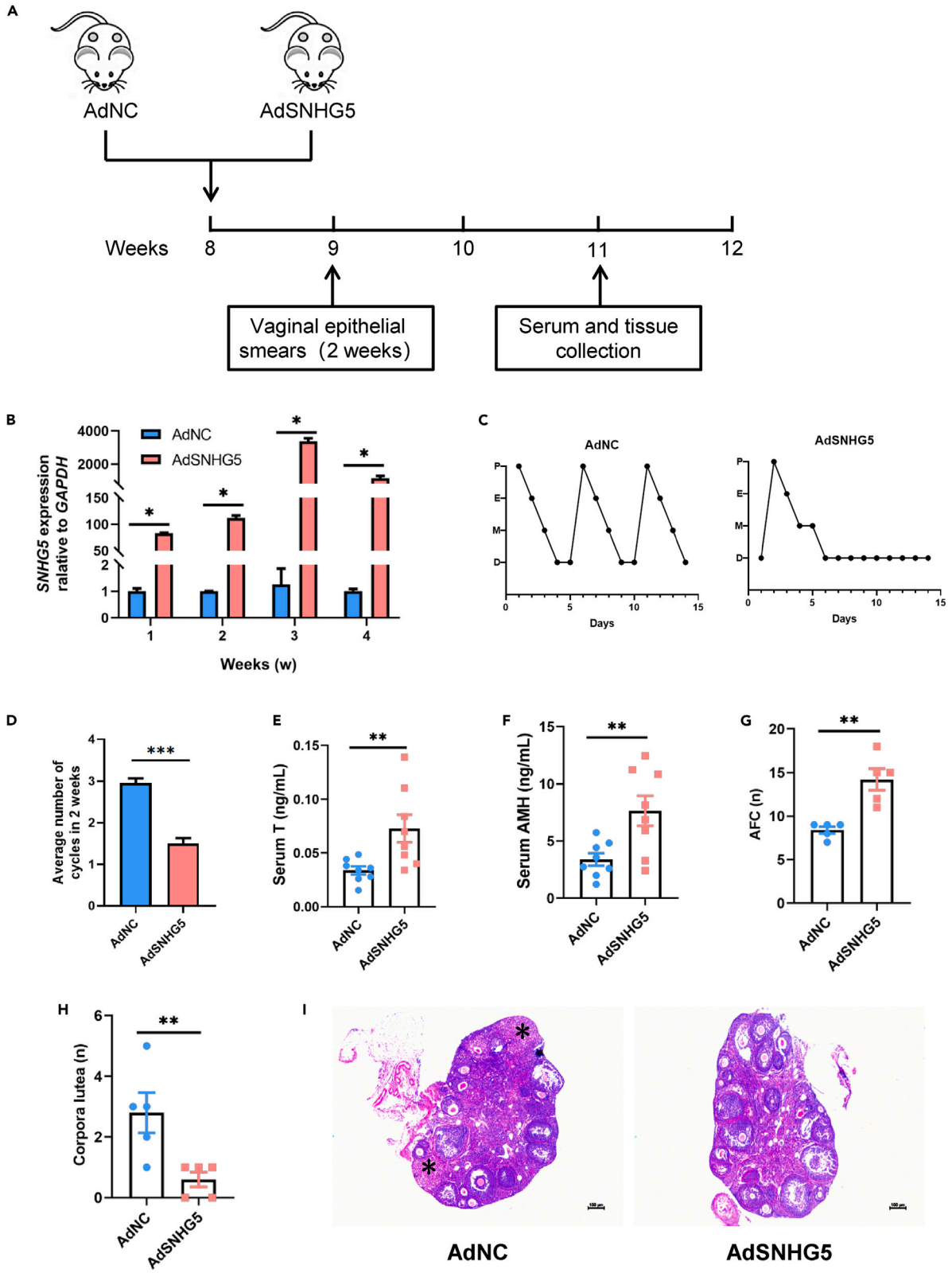
A
AdNC
AdSNHG5
Weeks
8
9
10
11
12
Vaginal epithelial smears (2 weeks)
Serum and tissue collection
B
AdNC
AdSNHG5
SNHG5 expression ralative to GAPDH
Weeks (w)
C
AdNC
AdSNHG5
P
E
M
D
Days
D
Average number of cycles in 2 weeks
E
Serum T (ng/mL)
F
Serum AMH (ng/mL)
G
AFC (n)
H
Corpora lutea (n)
I
AdNC
AdSNHG5

Figure 2. Overexpression of lncRNA SNHG5 induces PCOS-like features in mice

(A) Experimental design of the animal study. Female C57BL/6 mice aged 8 weeks were bilaterally injected with either recombinant adenovirus carrying human lncRNA SNHG5 (AdSNHG5) or an empty adenovirus vector (AdNC). The estrous cycle was assessed before sample collection of serum and tissues at 11 weeks of age.

(B) Successful overexpression of human lncRNA SNHG5 in mouse ovaries at 1–4 weeks after injection of the virus was confirmed by RT-qPCR. n = 3 per group.

(C) Representative estrous cycles during 14 consecutive days. P, proestrus; E, estrus; M, metestrus; D, diestrus.

(D) Average number of cycles during 14 consecutive days. n = 10 per group.

(E and F) Serum levels of testosterone (T) and anti-Mullerian hormone (AMH). n = 8 per group.

(G and H) Quantitative analysis of antral follicle count (AFC) and corpora lutea. n = 5 per group.

(I) Hematoxylin and eosin staining of representative ovaries.

* denotes corpora lutea. Scale bar: 100 μm. Images are representative of three independent experiments with similar results. Data in (B) and (D–H) are presented as mean ± SEM. Statistical significance was determined using a two-tailed t test. *p < 0.05; **p < 0.01; ***p < 0.001.

SNHG1, *SNHG2*, *SNHG5*, *SNHG7*, *SNHG8*, *SNHG9*, *SNHG15*, *SNHG16*, *SNHG17*, *SNHG19*, *SNHG21*, and *SNHG25* in GCs of PCOS women compared to controls (Figure 1A), indicating their potential involvement in the pathogenesis of PCOS. Among these transcripts, lncRNA SNHG5 exhibited the highest upregulation and was identified as being overexpressed in the GCs of PCOS women in our previous RNA-seq data,[17] which led us to focus our study on the potential role of SNHG5 in PCOS. Additionally, using data from National Center for Biotechnology Information (NCBI), we observed that SNHG5 is relatively highly expressed in human ovaries. Further validation of SNHG5's elevated expression in PCOS was done in cohort 2 (60 PCOS women and 60 controls), which demonstrated that the median expression level of SNHG5 was 2.1-fold higher ($p < 0.001$) in the GCs of PCOS women than that of controls (Figure 1B). Spearman correlation analysis revealed the expression level of SNHG5 was significantly correlated with antral follicle count (AFC) in women with PCOS (Figure 1C), but not with serum testosterone (T) levels (Figure 1D). These findings suggest that SNHG5 may play a role in the abnormal folliculogenesis in PCOS.

Overexpression of SNHG5 induces PCOS-like features in mice

To evaluate the potential role of lncRNA SNHG5 in the pathogenesis of PCOS, a mouse model was constructed via bilateral intraovarian injection of either recombinant adenovirus carrying human lncRNA SNHG5 (AdSNHG5) or an empty adenovirus vector (AdNC) (Figure 2A). Successful overexpression of SNHG5 in the ovaries of mice in the AdSNHG5 group was confirmed using RT-qPCR (Figure 2B). Compared with mice injected with empty vector, AdSNHG5-injected mice exhibited disturbed estrous cycles (Figures 2C and 2D), as well as elevated serum levels of T (Figure 2E) and anti-Mullerian hormone (AMH) (Figure 2F). Histological examination of ovarian sections revealed an accumulation of antral follicles (Figure 2G) and a decrease of corpora lutea (CL) (Figure 2H) in AdSNHG5-injected mice. The representative ovarian sections stained with H & E in both groups are shown in Figure 2I. Collectively, overexpression of SNHG5 in mice can induce disruption of estrous cycles, hyperandrogenism, elevated AMH levels, and polycystic ovarian morphology, all of which are hallmarks of PCOS.

LncRNA SNHG5 suppresses proliferation and promotes apoptosis of ovarian granulosa cells *in vitro*

Next, we investigated the effect of lncRNA SNHG5 on the proliferation and apoptosis of primary GCs and human ovarian granulosa tumor cell line (KGN) cells. The expression of follicle-stimulating hormone receptor (FSHR) was used to identify the primary GCs (Figure S1). Adenovirus carrying SNHG5 was introduced to overexpress SNHG5 in ovarian GCs, and two independent small interfering RNAs (siRNAs) against SNHG5 (siSNHG5-1 and siSNHG5-2) were applied to knockdown SNHG5 *in vitro*. The efficiency of overexpression and knockdown of SNHG5 was confirmed by RT-qPCR (Figures 3A and 3B). Cell Counting Kit-8 (CCK-8) and ethynyl-2-deoxyuridine (EdU) assays consistently showed that SNHG5 overexpression significantly inhibited the proliferation of KGN cells (Figures 3C and 3E), while silencing SNHG5 significantly prompted KGN cell proliferation (Figures 3D and 3F). Flow cytometry analysis revealed that SNHG5 overexpression increased the percentage of apoptotic cells in GCs and KGN cells (Figure 3G), while SNHG5 knockdown reduced it (Figure 3H). In addition, overexpression of SNHG5 in GCs and KGN cells led to elevated pro-apoptotic protein Bax and decreased anti-apoptotic protein Bcl-2 expression levels (Figure 3I). In contrast, SNHG5 knockdown led to decreased Bax and increased Bcl-2 expression levels (Figure 3J). Flow cytometry analysis of cell cycle progression revealed that SNHG5 overexpression induced more cells arrest at G0/G1 phase and reduced the proportion of cells at S phase (Figure 3K), whereas SNHG5 knockdown exhibited the opposite phenotype (Figure 3L). Taken together, these findings demonstrate that lncRNA SNHG5 inhibits cell proliferation and cell cycle progression, and induces apoptosis in ovarian GCs.

SNHG5 modulates multiple signaling pathways involved in DNA replication and repair

In order to investigate the biological effects of SNHG5, RNA-seq was performed to analyze the gene expression profiles affected by SNHG5 knockdown in KGN cells. A total of 77 upregulated genes and 257 downregulated genes were identified in KGN cells transfected with siSNHG5-1 compared to the control group (SiNC) (Figure 4A). GSEA revealed that SNHG5 knockdown predominantly affected DNA replication and repair mechanisms, as indicated by the top 8 highest-scoring signaling pathways (Figure 4B). Specifically, SNHG5 knockdown promoted DNA replication and double-strand break repair while inhibiting cell apoptosis (Figure 4C). Heat maps of representative genes involved in these signaling pathways are shown in the lower part of Figure 4C. Furthermore, RT-qPCR confirmed the dysregulated expression

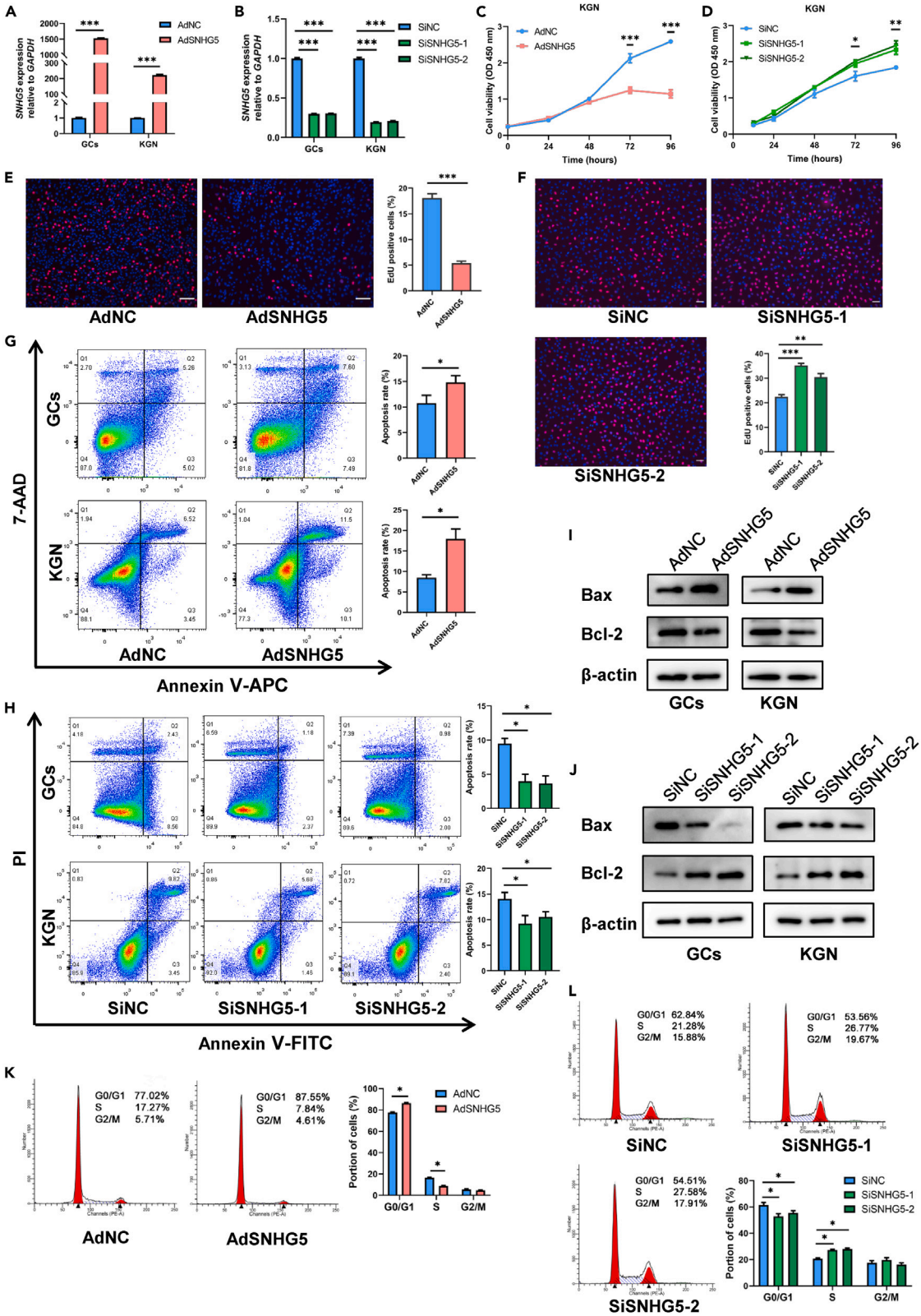
A
SNHG5 expression relative to GAPDH
AdNC
AdSNHG5
GCs
KGN
B
SNHG5 expression relative to GAPDH
SiNC
SiSNHG5-1
SiSNHG5-2
C
KGN
Cell viability (OD 450 nm)
Time (hours)
D
KGN
E
EdU positive cells (%)
F
G
7-AAD
Annexin V-APC
Apoptosis rate (%)
H
PI
Annexin V-FITC
I
Bax
Bcl-2
β-actin
J
K
G0/G1 77.02%
S 17.27%
G2/M 5.71%
G0/G1 87.55%
S 7.84%
G2/M 4.61%
Portion of cells (%)
L
G0/G1 62.84%
S 21.28%
G2/M 15.88%
G0/G1 53.56%
S 26.77%
G2/M 19.67%
G0/G1 54.51%
S 27.58%
G2/M 17.91%

Figure 3. LncRNA SNHG5 suppresses cell proliferation and cell cycle progression and induces apoptosis *in vitro*

(A and B) SNHG5 expression was evaluated by RT-qPCR in primary granulosa cells (GCs) and KGN cells infected with adenovirus expressing SNHG5 or an empty vector (A), or two different siRNAs against SNHG5 or mock control (B).

(C and D) The proliferation of KGN cells was assessed using the CCK-8 assay following adenoviral infection with either AdSNHG5 or AdNC (C), or transfection with SNHG5 siRNAs or mock control (D).

(E and F) The proliferation of KGN cells was assessed using the EdU assay following adenoviral infection with either AdSNHG5 or AdNC (E), or transfection with SNHG5 siRNAs or the control (F).

(G and H) Apoptosis was detected by flow cytometry in GCs and KGN cells infected with AdSNHG5 or AdNC (G), or transfected with SNHG5 siRNAs or the control (H).

(I and J) Western blot analysis of protein expression levels of Bax and Bcl-2 in GCs and KGN cells infected with AdSNHG5 or AdNC (I), or transfected with SNHG5 siRNAs or the control (J).

(K and L) Flow cytometry was used to investigate the effect of SNHG5 on cell cycle distribution in KGN cells after overexpressing SNHG5 (K) or knockdown SNHG5 (L).

The data were presented as the mean ± SEM obtained from at least three independent experiments. Statistical significance was determined using either Student's *t* test or one-way ANOVA as appropriate. *$p < 0.05$; **$p < 0.01$; ***$p < 0.001$.

of genes related to cell proliferation, apoptosis, and cell cycle progression after SNHG5 knockdown in KGN cells (Figure 4D), which was consistent with the RNA-seq results. These findings suggest that SNHG5 may exert its anti-proliferation and pro-apoptosis effects through modulating cell cycle, proliferation, and apoptosis pathways in KGN cells.

SNHG5 functions as a molecular sponge for miR-92a-3p in KGN cells

To further investigate the mechanism by which SNHG5 regulates the proliferation and apoptosis of GCs, we first examined the subcellular localization of SNHG5 in these cells. As revealed by RNA-fluorescence *in situ* hybridization (FISH) (Figure 5A) and subcellular fractionation by RT-qPCR (Figure 5B), SNHG5 is predominantly expressed in the cytoplasm of both primary GCs and KGN cells. Many cytoplasmic lncRNAs have been reported to act as competing endogenous RNAs (ceRNAs) by competitively binding to microRNAs (miRNAs).[22] To identify the miRNA(s) interacting with SNHG5, Starbase and miRcode were used to predict miRNAs containing binding sites for SNHG5. We obtained 14 potential target miRNAs after intersection analysis (Figure S2). Although these 14 miRNAs were detected by RT-qPCR in KGN cells overexpressing SNHG5, only 6 miRNAs were satisfactorily amplified, which demonstrated that miR-92a-3p and miR-212-3p were significantly downregulated (Figure 5C). MiR-92a-3p, a miRNA that has been reported to function as an oncogene in various cancers,[23] was further investigated. Argonaute 2 (Ago2) is a critical component of the RNA-induced silencing complex (RISC), which is essential for miRNA-mediated gene silencing.[24] RNA immunoprecipitation (RIP) assays showed that SNHG5 and miR-92a-3p were prominently enriched in Ago2-containing micro-ribonucleoprotein complexes (Figure 5D), indicating that they are a part of the same RISC. RNAhybrid 2.2 software was utilized to predict the putative binding sites of SNHG5 with miR-92a-3p, revealing 4 potential binding sites (Figure S3). We then constructed different luciferase reporter vectors based on SNHG5 wild-type (SNHG5-wt) and mutant type sequences (SNHG5-mut1, SNHG5-mut2, SNHG5-mut3, and SNHG5-mut4), which were mutated in the binding sites for miR-92a-3p (Figure S3). These vectors were subjected to dual luciferase reporter assays, which demonstrated that miR-92a-3p overexpression significantly reduced the luciferase activity of the vectors containing SNHG5-wt, SNHG5-mut1, SNHG5-mut3, and SNHG5-mut4 but not SNHG5-mut2 (Figure 5E). This indicates that nt 175–208 of SNHG5 is the target binding site of miR-92a-3p. RT-qPCR analysis revealed that miR-92a-3p negatively regulated SNHG5 expression in KGN cells (Figure 5F). In functional assays, we found that miR-92a-3p overexpression in KGN cells attenuated the growth inhibition effect of SNHG5 (Figures 5G and 5H). Flow cytometry analysis (Figure 5I) and WB data (Figure 5J) confirmed that miR-92a-3p overexpression could rescue SNHG5-mediated apoptosis. Furthermore, miR-92a-3p mimics reversed cell-cycle arrest at G1 stage induced by SNHG5 overexpression in KGN cells (Figure 5K). In cohort 3 consisting of 30 PCOS women and 30 controls, we found that miR-92a-3p was downregulated in GCs from PCOS women compared to controls (Figure 5L). Notably, Spearman correlation analysis revealed an inverse correlation between the expression levels of SNHG5 and miR-92a-3p in GCs of PCOS women (Figure 5M). Overall, these results provided strong evidence that SNHG5 plays a critical role in suppressing proliferation while promoting apoptosis in KGN cells through acting as a molecular sponge for miR-92a-3p.

CDKN1C is a target of miR-92a-3p

To elucidate the mechanism underlying the regulation of proliferation and apoptosis by miR-92a-3p in ovarian GCs, we utilized starBase v2.0 to predict potential target genes and obtained 236 candidates by intersecting the results of four different databases (targetScan, picTar, PITA, and miRanda/mirSVR). Then, we further narrowed the list by finding the intersection of these 236 candidates with the 257 genes significantly downregulated by the knockdown of SNHG5, as revealed by RNA-seq. Ultimately, we identified three potential target genes: cyclin dependent kinase (CDK) inhibitor 1C (*CDKN1C*, p57KIP2), CCAAT enhancer binding protein alpha (*CEBPA*), and glutamine-fructose-6-phosphate transaminase 2 (*GFPT2*). *CDKN1C* is well-established as a cyclin-dependent kinase inhibitor and negative regulator of cell proliferation.[25] Bioinformatics analysis indicated that both SNHG5 and CDKN1C 3′ untranslated region (3′ UTR) share a consensus binding site for miR-92a-3p, suggesting SNHG5's potential to act as a ceRNA to exert its regulatory effect. Confirming these findings, RT-qPCR and WB experiments demonstrated that miR-92a-3p mimics significantly inhibited the expression of CDKN1C, while miR-92a-3p inhibitor displayed the opposite effect (Figure 6A). We also found that the transcription of CDKN1C increased and decreased in KGN cells after overexpression and knockdown of SNHG5, respectively (Figure 6B). Dual luciferase reporter assays (Figure 6C) additionally revealed that miR-92a-3p mimics reduced

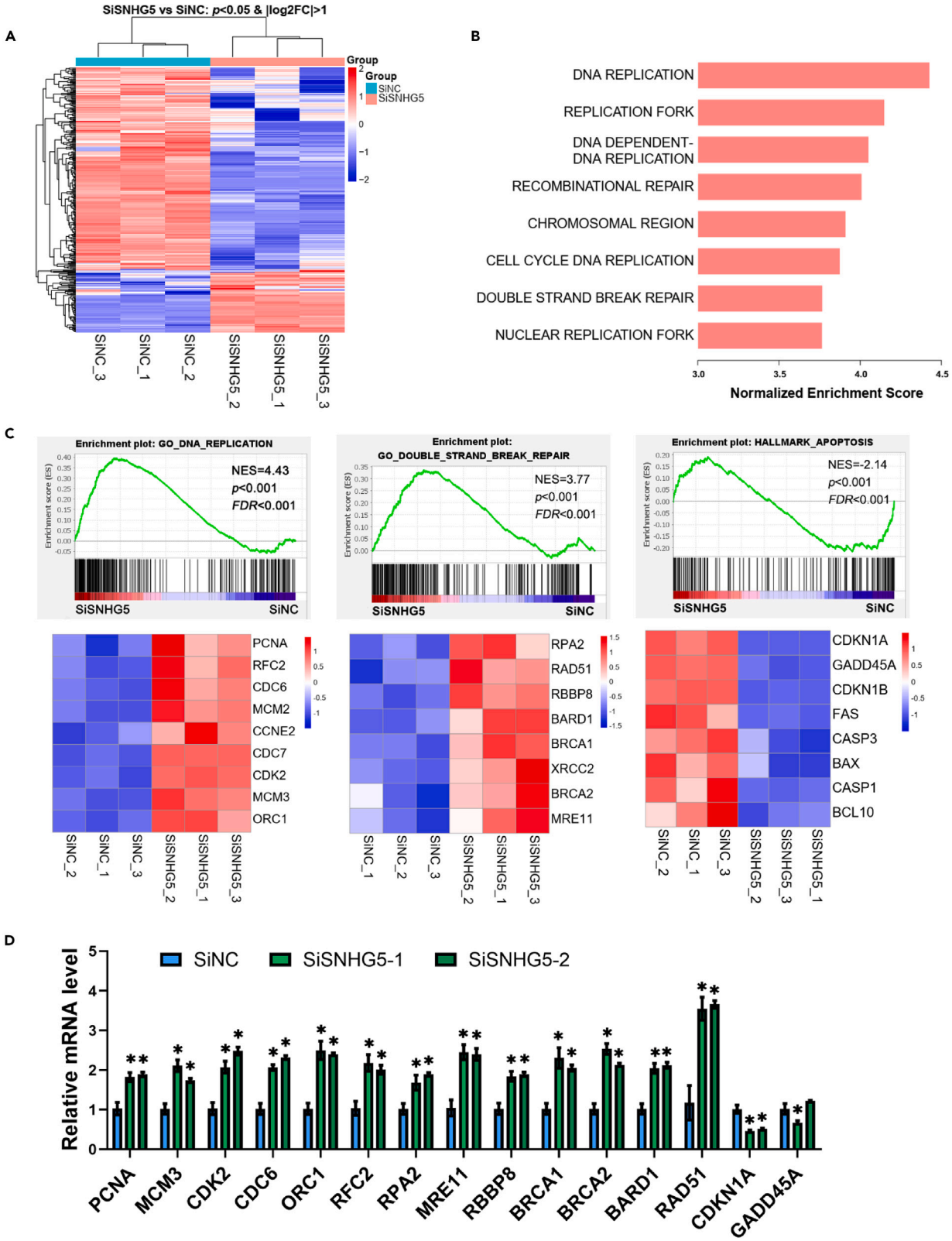
A
SiSNHG5 vs SiNC: p<0.05 & |log2FC|>1
Group
SiNC
SiSNHG5
SiNC_3
SiNC_1
SiNC_2
SiSNHG5_2
SiSNHG5_1
SiSNHG5_3
B
DNA REPLICATION
REPLICATION FORK
DNA DEPENDENT-DNA REPLICATION
RECOMBINATIONAL REPAIR
CHROMOSOMAL REGION
CELL CYCLE DNA REPLICATION
DOUBLE STRAND BREAK REPAIR
NUCLEAR REPLICATION FORK
3.0
3.5
4.0
4.5
Normalized Enrichment Score
C
Enrichment plot: GO_DNA_REPLICATION
NES=4.43
p<0.001
FDR<0.001
Enrichment plot:
GO_DOUBLE_STRAND_BREAK_REPAIR
NES=3.77
p<0.001
FDR<0.001
Enrichment plot: HALLMARK_APOPTOSIS
NES=-2.14
p<0.001
FDR<0.001
SiSNHG5
SiNC
PCNA
RFC2
CDC6
MCM2
CCNE2
CDC7
CDK2
MCM3
ORC1
RPA2
RAD51
RBBP8
BARD1
BRCA1
XRCC2
BRCA2
MRE11
CDKN1A
GADD45A
CDKN1B
FAS
CASP3
BAX
CASP1
BCL10
D
SiNC
SiSNHG5-1
SiSNHG5-2
Relative mRNA level
PCNA
MCM3
CDK2
CDC6
ORC1
RFC2
RPA2
MRE11
RBBP8
BRCA1
BRCA2
BARD1
RAD51
CDKN1A
GADD45A

Figure 4. SNHG5 knockdown causes deregulation of genes involved in DNA replication and repair in KGN cells

(A) Heatmap displaying gene expression profiles of KGN cells transfected with SiSNHG5-1 or the mock control. Gene expression levels are represented by a color-coded scale, with blue, white, and red indicating low, intermediate, and high expression, respectively.

(B) The top 8 significantly enriched ontology gene sets ranked by normalized enrichment score in KGN cells affected by SNHG5 knockdown.

(C) The upper half of the panel shows the GSEA plots of pathways involved in DNA replication, DNA double-strand break repair, and apoptosis in KGN cells with SNHG5 knockdown. The lower half shows the heatmap of select genes from these pathways, with blue, white, and red colors indicating low, intermediate, and high expression levels, respectively.

(D) RT-qPCR for selected genes from the ranked pathways in KGN cells transfected with SNHG5 siRNAs.

Data are presented as the mean ± SEM from three independent experiments. Statistical significance was determined using a two-tailed unpaired t test. *$p < 0.05$.

the luciferase activities of the reporter plasmid harboring the CDKN1C 3′ UTR sequence with the putative binding site for miR-92a-3p (p57-wt), and mutation of the binding site (p57-mut) abolished the inhibitory effect of miR-92a-3p on CDKN1C. Importantly, SNHG5 overexpression was shown to rescue the inhibitory effect of miR-92a-3p on CDKN1C 3′ UTR luciferase reporter (Figure 6C). To confirm that SNHG5 regulated CDKN1C by acting as a miRNA sponge for miR-92a-3p, we examined the protein expression levels of CDKN1C. As shown in Figure 6D, overexpression of SNHG5 significantly promoted p57 expression, which was significantly attenuated by miR-92a-3p overexpression. This indicates that SNHG5 regulates CDKN1C expression in a miR-92a-3p-dependent manner. Furthermore, we observed that the expression level of CDKN1C was significantly higher in GCs of PCOS women compared to that of control women (Figure 6E). As expected, the expression of CDKN1C was negatively correlated with miR-92a-3p and positively correlated with SNHG5 in GCs of PCOS women (Figures 6F and 6G). Our results indicate that CDKN1C is a direct target of miR-92a-3p and that SNHG5 may exert its function through the miR-92a-3p/CDKN1C axis.

DISCUSSION

In this study, we found that lncRNA SNHG5 was significantly upregulated in GCs of PCOS women, and that its expression level positively correlated with AFC in these women. Our *in vivo* experiments using mouse models showed SNHG5 could induce PCOS-like features, while *in vitro* studies demonstrated that SNHG5 could suppress proliferation, promote apoptosis, and induce cell-cycle arrest at the G0/G1 stage in GCs by acting as a sponge for miR-92a-3p. Further investigations revealed that miR-92a-3p targeted CDKN1C. Thus, this study presents evidence for the first time that lncRNA SNHG5 can suppress proliferation and promote apoptosis of GCs by regulating the miR-92a-3p/CDKN1C axis.

It has been recognized that the distinctive features of folliculogenesis in PCOS include an increase of growing preantral follicles and arrest of follicle development beyond mid-antral stage.[6] Nevertheless, the mechanisms responsible for these phenomena remain unclear. As GCs provide nutrients and growth factors for oocytes, proper proliferation and apoptosis of GCs are essential for follicle development. However, there is controversy regarding changes in the proliferation and apoptosis of GCs in PCOS. Stubbs et al.[26] and Das et al.[27] reported increased proliferation and decreased apoptosis of GCs in early growing follicles of PCOS women. In contrast, Zhao et al.[28] found the expression level of the cell proliferation marker proliferating cell nuclear antigen (PCNA) was significantly lower in GCs of PCOS women than in those of control women, and several studies[29–33] demonstrated a significantly increased apoptosis rate of GCs in women with PCOS. This difference may be attributed to the follicles of different development stages. Das[27] and Stubbs[26] primarily investigated small follicles in the early growth stage, whereas Zhao et al.[28] and the other several studies[29–33] primarily investigated luteinized large follicles. We speculate that GCs undergo biphasic alterations in proliferation and apoptosis in PCOS, namely increased proliferation and decreased apoptosis in small follicles and decreased proliferation and increased apoptosis in large follicles. Supporting this hypothesis, Stubbs et al.[26] observed a lower but nonsignificant tendency of GC proliferation in the secondary follicles of PCOS women than in those of controls. This aforementioned hypothesis is also consistent with the stage-specific regulation of follicle growth by excess androgens, another important characteristic of PCOS, which promotes pre-antral follicle growth but inhibits follicular development of later stages.[13,34–36] The GCs investigated in this study were derived from luteinized large follicles. Our data suggest decreased proliferation and increased apoptosis of GCs in PCOS women, in agreement with this hypothesis.

SNHG5 is a member of the non-protein-coding SNHG family and was first discovered in 2000 by Tanaka et al. at a breakpoint of chromosomal translocation involved in human B-cell lymphoma.[37] In recent years, aberrant expression of SNHG5 has been documented in multiple tumors, where it shows strong correlations with clinicopathological features, metastasis, and prognosis.[38–41] SNHG5 has demonstrated tumor-suppressor or oncogenic functions in various tumors. For instance, it exerts pro-tumor effects in liver[42] and lung cancer[40] and has anti-tumor properties in endometrial[43] and ovarian cancer.[44] Mechanism investigations have revealed that SNHG5 participates in a variety of cellular activities, such as proliferation, apoptosis, invasion, migration, cell-cycle regulation, autophagy, fibrosis, and inflammation, through the regulation of miRNAs, signaling pathways, as well as other proteins or molecules.[38–41,45,46] Despite the known involvement of SNHG5 in numerous tumors, its role and mechanism have not been reported in PCOS. Two studies have reported a tumor suppressive effect of SNHG5 in ovarian cancer,[44,47] consistent with the anti-proliferative and pro-apoptotic effects of SNHG5 in GCs observed in this study.

Our *in vivo* experiments revealed that SNHG5 could induce PCOS-like features in mice, while *in vitro* studies demonstrated that it inhibited GC proliferation and induced apoptosis and cell-cycle arrest at G0/G1 phase. Subcellular localization analysis showed that SNHG5 was predominantly located in the cytoplasm of GCs. One function of cytoplasmic lncRNAs is to act as ceRNAs by binding to shared miRNAs, thereby reducing miRNA availability and modulating mRNA expression.[22] Our in silico analysis and functional experiments identified miR-92a-3p as a

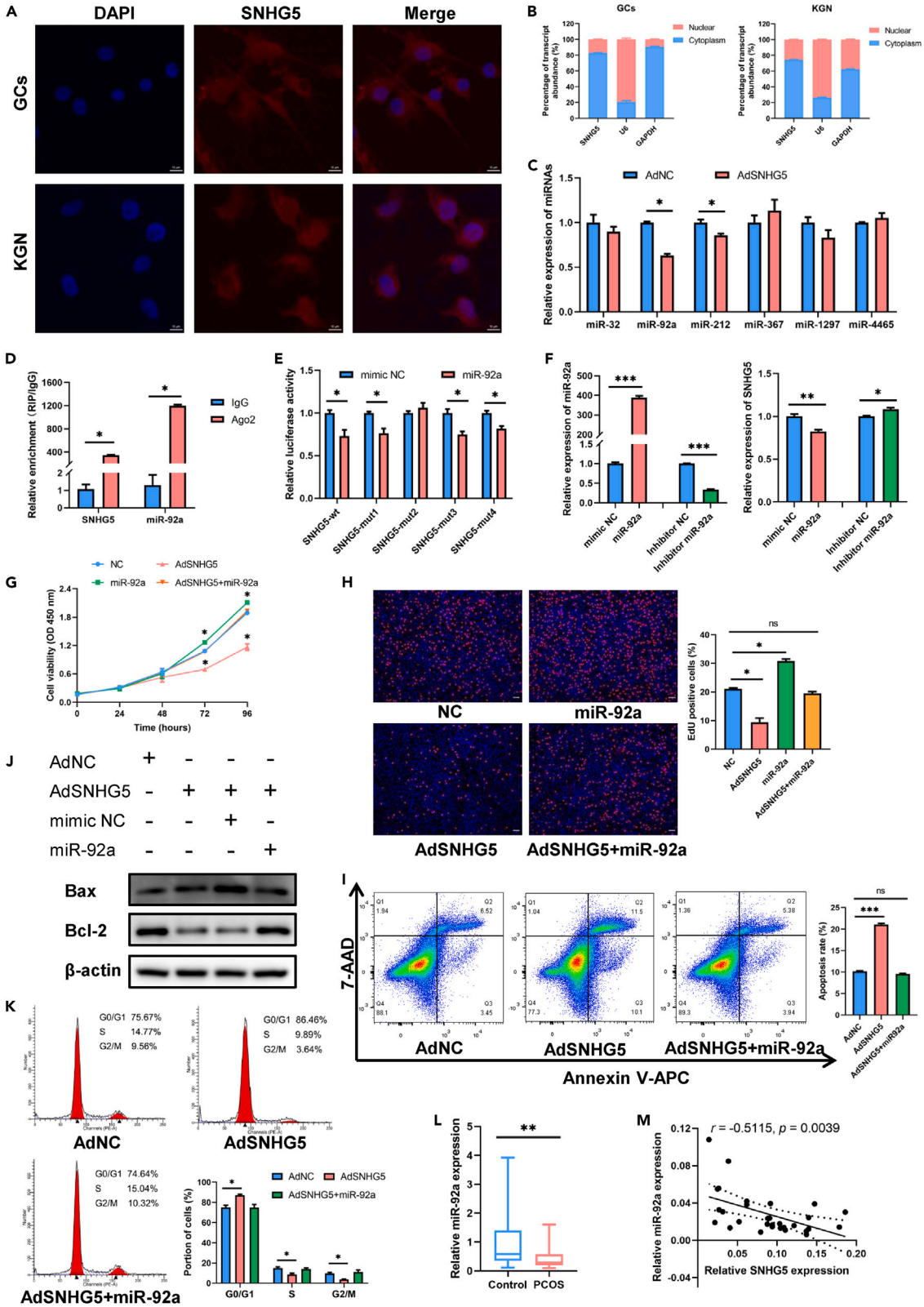
A
DAPI
SNHG5
Merge
GCs
KGN
B
GCs
KGN
Nuclear
Cytoplasm
Percentage of transcript abundance (%)
SNHG5
U6
GAPDH
C
AdNC
AdSNHG5
Relative expression of miRNAs
miR-32
miR-92a
miR-212
miR-367
miR-1297
miR-4465
D
IgG
Ago2
Relative enrichment (RIP/IgG)
SNHG5
miR-92a
E
mimic NC
miR-92a
Relative luciferase activity
SNHG5-wt
SNHG5-mut1
SNHG5-mut2
SNHG5-mut3
SNHG5-mut4
F
Relative expression of miR-92a
Relative expression of SNHG5
mimic NC
miR-92a
Inhibitor NC
Inhibitor miR-92a
G
NC
AdSNHG5
miR-92a
AdSNHG5+miR-92a
Cell viability (OD 450 nm)
Time (hours)
H
NC
miR-92a
AdSNHG5
AdSNHG5+miR-92a
EdU positive cells (%)
ns
J
AdNC
AdSNHG5
mimic NC
miR-92a
Bax
Bcl-2
β-actin
I
7-AAD
Annexin V-APC
AdNC
AdSNHG5
AdSNHG5+miR-92a
Apoptosis rate (%)
K
G0/G1 75.67%
S 14.77%
G2/M 9.56%
AdNC
G0/G1 86.46%
S 9.89%
G2/M 3.64%
AdSNHG5
G0/G1 74.64%
S 15.04%
G2/M 10.32%
AdSNHG5+miR-92a
Portion of cells (%)
G0/G1
S
G2/M
L
Relative miR-92a expression
Control
PCOS
M
r = -0.5115, p = 0.0039
Relative miR-92a expression
Relative SNHG5 expression

Figure 5. SNHG5 functions as a molecular sponge for miR-92a-3p in KGN cells

(A) RNA-FISH was performed to visualize SNHG5 expression (red) and nuclei (blue) in GCs and KGN cells. Scale bar: 10 μm.

(B) RNA was extracted from the nuclear and cytosolic fractions of GCs and KGN cells to quantify SNHG5 levels using RT-qPCR. U6 and GAPDH were used as nuclear and cytosolic controls, respectively.

(C) The expression of a panel of miRNAs including miR-32-5p, miR-92a-3p, miR-212-3p, miR-367-3p, miR-1297, and miR-4465 were analyzed by RT-PCR in KGN cells infected with AdSNHG5 or AdNC.

(D) RNA immunoprecipitation analysis of endogenous Ago2 binding to RNA in KGN cells, where IgG was used as the control. SNHG5 and miR-92a-3p levels were determined by qRT-PCR and presented as fold enrichment in Ago2 relative to input.

(E) Relative luciferase activities of wild type (wt) and mutated (mut) SNHG5 reporter plasmids in HEK293 cells co-transfected with miR-92a-3p mimics.

(F) Relative expression of miR-92a-3p and SNHG5 in KGN cells transfected with mimics or inhibitor of miR-92-3p or the control.

(G and H) CCK-8 (G) and EdU (H) assays showed proliferation reduction caused by SNHG5 overexpression could be counteracted by miR-92a-3p mimics in KGN cells.

(I and J) Flow cytometry (I) and Western blot (J) experiments showed cell apoptosis induced by SNHG5 overexpression could be reduced by miR-92a-3p mimics in KGN cells. Images in (J) are representative of three independent experiments with similar results.

(K) Cell cycle recue experiments demonstrated that cell cycle inhibition induced by SNHG5 overexpression could be attenuated by miR-92a-3p mimics in KGN cells.

(L) Relative miR-92a-3p expression levels in GCs from 30 PCOS women and 30 controls (cohort 3).

(M) Spearman correlation analysis of expression levels between SNHG5 and miR-92a-3p in GCs from 30 PCOS women.

Data in (B–I) and (K and L) were presented as the mean ± SEM obtained from three independent experiments. Statistical significance was determined using either Student's *t* test or one-way ANOVA as appropriate. *$p < 0.05$; **$p < 0.01$; ***$p < 0.001$.

ceRNA of SNHG5. MiR-92a-3p has been reported to promote proliferation and suppress apoptosis in multiple cancers,[23,48,49] as well as inhibit porcine ovarian GCs apoptosis,[49] consistent with our findings. Additionally, Lin et al.[50] demonstrated downregulated miR-92a and miR-92b in ovarian theca interna tissues of PCOS women. Furthermore, it has been reported that miR-92a-3p plays a critical role in FSH-mediated Sertoli cells maturation and male fertility.[51] As Sertoli cells and GCs share a common embryological origin,[52] it is worthwhile to explore whether miR-92a-3p plays an important role in ovarian folliculogenesis and ovulation.

Further investigations revealed that miR-92a-3p targets CDKN1C to regulate GCs proliferation and apoptosis. MiR-92a-3p has also been reported to suppress proliferation and stimulate apoptosis in human colon cancer cells by targeting CDKN1C.[53] *CDKN1C* is a paternally imprinted gene with preferential expression of the maternal allele.[54] Mutations in *CDKN1C* are implicated in Beckwith-Wiedemann syndrome and sporadic cancers, emphasizing its potential as a tumor suppressor candidate.[25] The protein encoded by *CDKN1C*, p57KIP2, belongs to the Cip/Kip family, which also includes p27KIP1 and p21CIP1/WAF1.[54] These proteins inhibit cyclin/CDK complexes to halt cell cycle progression and induce G0/G1 phase arrest, leading to suppressed cell proliferation and activated apoptosis pathways.[54] Although the role of CDKN1C in PCOS has not been elucidated, the inhibitory effect of its family member proteins, p27KIP1 and p21CIP1/WAF1, on cell proliferation in the GCs of women with PCOS has been reported.[12,28,55] Consistent with these findings, we observed KGN cells overexpressing SNHG5 showed G0/G1 phase arrest, reduced proliferation, and increased apoptosis, supporting SNHG5 may function through the miR-92a-3p/CDKN1C axis. RNA-seq analysis demonstrated SNHG5 knockdown mainly affects DNA synthesis signaling pathways, providing additional support for *CDKN1C* as the downstream target gene. Moreover, p57Kip2-deficient mice have been found to exhibit immaturity of germinal tissues including ovaries, uterus, testes and prostate,[56] highlighting the crucial role of p57KIP2 in reproductive system development.

In summary, our results demonstrate that the aberrant overexpression of lncRNA SNHG5 in GCs of PCOS women may adversely impact folliculogenesis. Specifically, SNHG5 functions as a ceRNA to sequester miR-92a-3p, leading to elevated expression of CDKN1C and ultimately causing suppressed proliferation and increased apoptosis in ovarian GCs. These findings suggest that SNHG5 has the potential to serve as both a novel diagnostic biomarker and a therapeutic target for PCOS.

Limitations of the study

This study has several limitations that should be acknowledged. First, the GCs used in this study are collected following gonadotropin stimulation and the induction of an ovulatory process, thus representing luteinized GCs. Although widely used, the transcriptional pattern of luteinized GCs is distinct from that of GCs during the follicular phase, and its relevance to *in vivo* mechanisms of follicular development remains a topic of debate. Regrettably, it is currently not feasible to collect non-luteinized GCs. To address this limitation to some extent, KGN cells were employed in this study. Second, the cause of SNHG5 overexpression in PCOS was not addressed in this study. Further research is warranted to elucidate the molecular mechanisms of SNHG5 dysregulation in PCOS.

STAR★METHODS

Detailed methods are provided in the online version of this paper and include the following:

- KEY RESOURCES TABLE
- RESOURCE AVAILABILITY
  - Lead contact
  - Materials availability
  - Data and code availability

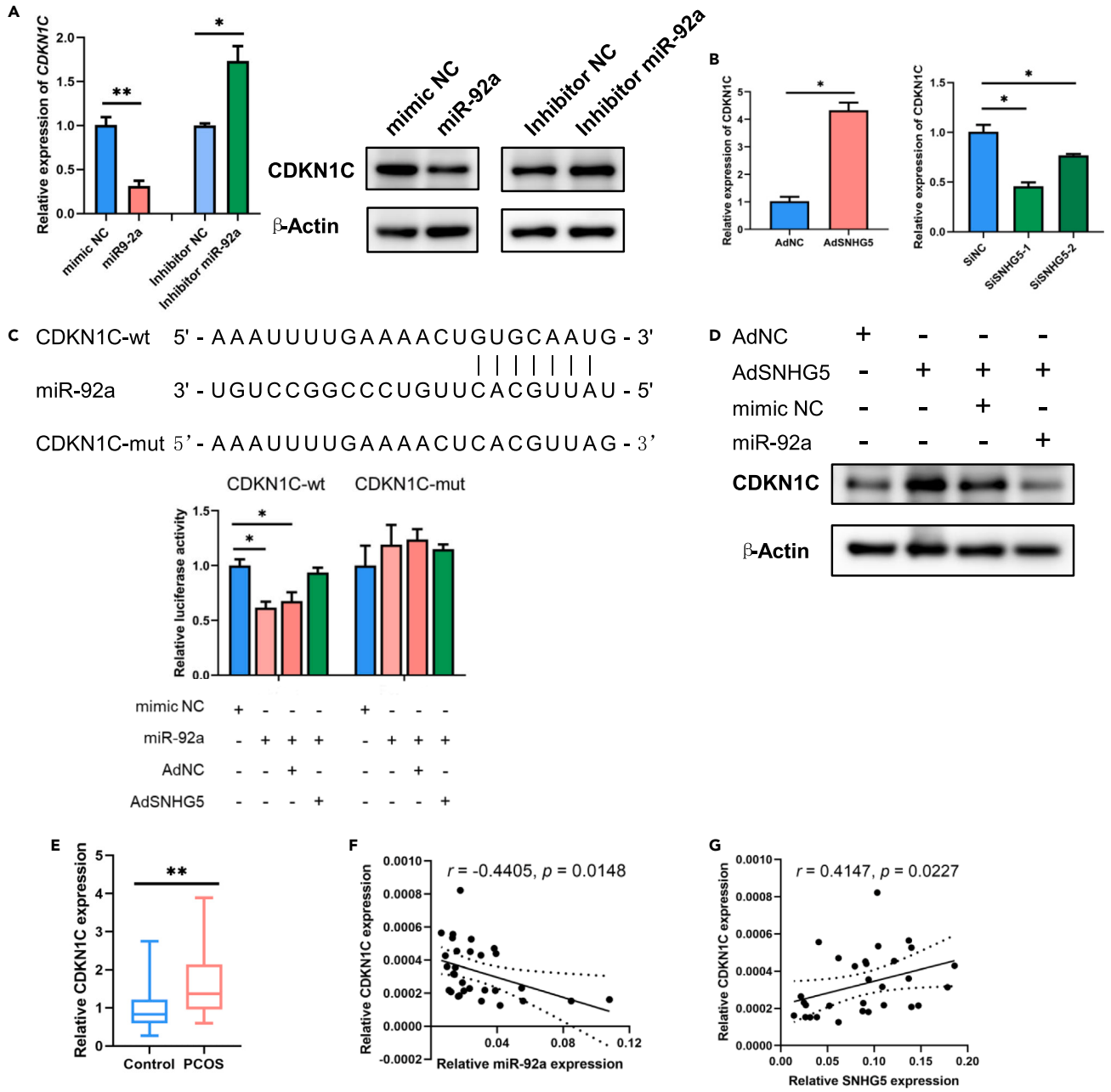

Figure 6. CDKN1C is a target of miR-92a-3p

(A) RT-qPCR and WB showed the relative expression of CDKN1C in KGN cells after miR-92a-3p was overexpressed or knocked down. The WB images are representative of three independent experiments with similar results.

(B) Relative expression of CDKN1C in KGN cells after overexpression or knockdown of SNHG5.

(C) Relative luciferase activities of wild type (wt) and mutant (mut) p57 reporter plasmids in HEK293 cells co-transfected with miR-92a-3p mimics, with or without AdSNHG5 infection.

(D) Overexpression of SNHG5 reduced the expression level of CDKN1C, and miR-92a-3p mimics were shown to reverse this effect in KGN cells. The images are representative of three independent experiments with similar results.

(E) Relative expression level of CDKN1C was measured by RT-qPCR in GCs from 30 PCOS women and 30 controls.

(F and G) Spearman correlation analyses were employed to determine the expression levels of CDKN1C with miR-92a-3p (F) and SNHG5 (G) in GCs from 30 PCOS women.

Data in (A–C) and (E) were presented as the mean ± SEM obtained from three independent experiments. Statistical significance was determined using either Student's *t* test or one-way ANOVA as appropriate. *p < 0.05; **p < 0.01.

SUPPLEMENTAL INFORMATION

Supplemental information can be found online at https://doi.org/10.1016/j.isci.2023.108522.

ACKNOWLEDGMENTS

This study was supported by National Natural Science Foundation of China (No.82088102 and No. 82171688), CAMS Innovation Fund for Medical Sciences (2019-I2M-5-064), Collaborative Innovation Program of Shanghai Municipal Health Commission (2020CXJQ01), Key Discipline Construction Project (2023–2025) of Three-Year Initiative Plan for Strengthening Public Health System Construction in Shanghai (GWVI-11.1-35), Clinical Research Plan of SHDC (SHDC2020CR1008A), Shanghai Clinical Research Center for Gynecological Diseases (22MC1940200), Shanghai Urogenital System Diseases Research Center (2022ZZ01012) and Shanghai Frontiers Science Research Center of Reproduction and Development.

AUTHOR CONTRIBUTIONS

Z.W.Y., J.X.P., and C.L.Z. conducted conception and design, collection and/or assembly of data, data analysis and interpretation, and manuscript writing. C.J.Y. and Z.Y.Z. conducted and assisted with experiments and data analysis and interpretation. G.L.D., X.M.L., and J.Z.S. assisted with experimental design, data analysis, and data interpretation. L.J. and H.F.H. provided conception and design, data analysis and interpretation, manuscript writing, and final approval of manuscript.

DECLARATION OF INTERESTS

The authors declare no competing interest. The graphical abstract was created with BioRender.com.

Received: August 14, 2023
Revised: November 13, 2023
Accepted: November 20, 2023
Published: November 23, 2023

REFERENCES

1. Escobar-Morreale, H.F. (2018). Polycystic ovary syndrome: definition, aetiology, diagnosis and treatment. Nat. Rev. Endocrinol. *14*, 270–284.
2. Rotterdam ESHRE/ASRM-Sponsored PCOS Consensus Workshop Group (2004). Revised 2003 consensus on diagnostic criteria and long-term health risks related to polycystic ovary syndrome. Fertil. Steril. *81*, 19–25.
3. Joham, A.E., Norman, R.J., Stener-Victorin, E., Legro, R.S., Franks, S., Moran, L.J., Boyle, J., and Teede, H.J. (2022). Polycystic ovary syndrome. Lancet Diabetes Endocrinol. *10*, 668–680.
4. Webber, L.J., Stubbs, S., Stark, J., Trew, G.H., Margara, R., Hardy, K., and Franks, S. (2003). Formation and early development of follicles in the polycystic ovary. Lancet (London, England) *362*, 1017–1021.
5. Franks, S., Stark, J., and Hardy, K. (2008). Follicle dynamics and anovulation in polycystic ovary syndrome. Hum. Reprod. Update *14*, 367–378.
6. Chang, R.J., and Cook-Andersen, H. (2013). Disordered follicle development. Mol. Cell. Endocrinol. *373*, 51–60.
7. Dompe, C., Kulus, M., Stefańska, K., Kranc, W., Chermuła, B., Bryl, R., Pieńkowski, W., Nawrocki, M.J., Petitte, J.N., Stelmach, B.,

et al. (2021). Human granulosa cells-stemness properties, molecular cross-talk and follicular angiogenesis. Cells *10*, 1396.
8. Matsuda, F., Inoue, N., Manabe, N., and Ohkura, S. (2012). Follicular growth and atresia in mammalian ovaries: regulation by survival and death of granulosa cells. J. Reprod. Dev. *58*, 44–50.
9. Regan, S.L.P., Knight, P.G., Yovich, J.L., Leung, Y., Arfuso, F., and Dharmarajan, A. (2018). Granulosa cell apoptosis in the ovarian follicle-a changing view. Front. Endocrinol. *9*, 61.
10. Wang, C., Sun, H., Davis, J.S., Wang, X., Huo, L., Sun, N., Huang, Q., Lv, X., Wang, C., He, C., et al. (2023). FHL2 deficiency impairs follicular development and fertility by attenuating EGF/EGFR/YAP signaling in ovarian granulosa cells. Cell Death Dis. *14*, 239.
11. McNatty, K.P., Smith, D.M., Makris, A., Osathanondh, R., and Ryan, K.J. (1979). The microenvironment of the human antral follicle: interrelationships among the steroid levels in antral fluid, the population of granulosa cells, and the status of the oocyte in vivo and in vitro. J. Clin. Endocrinol. Metab. *49*, 851–860.
12. Geng, X., Zhao, J., Huang, J., Li, S., Chu, W., Wang, W.S., Chen, Z.J., and Du, Y. (2021). lnc-MAP3K13-7:1 inhibits ovarian GC proliferation in PCOS via DNMT1 downregulation-mediated CDKN1A promoter hypomethylation. Mol. Ther. *29*, 1279–1293.
13. Azhary, J.M.K., Harada, M., Takahashi, N., Nose, E., Kunitomi, C., Koike, H., Hirata, T., Hirota, Y., Koga, K., Wada-Hiraike, O., et al. (2019). Endoplasmic reticulum stress activated by androgen enhances apoptosis of granulosa cells via induction of death receptor 5 in PCOS. Endocrinology *160*, 119–132.
14. Jiang, L., Huang, J., Li, L., Chen, Y., Chen, X., Zhao, X., and Yang, D. (2015). MicroRNA-93 promotes ovarian granulosa cells proliferation through targeting CDKN1A in polycystic ovarian syndrome. J. Clin. Endocrinol. Metab. *100*, E729–E738.
15. Andergassen, D., and Rinn, J.L. (2022). From genotype to phenotype: genetics of mammalian long non-coding RNAs in vivo. Nat. Rev. Genet. *23*, 229–243.
16. Mu, L., Sun, X., Tu, M., and Zhang, D. (2021). Non-coding RNAs in polycystic ovary syndrome: a systematic review and meta-analysis. Reprod. Biol. Endocrinol. *19*, 10.
17. Pan, J.X., Tan, Y.J., Wang, F.F., Hou, N.N., Xiang, Y.Q., Zhang, J.Y., Liu, Y., Qu, F., Meng, Q., Xu, J., et al. (2018). Aberrant expression and DNA methylation of lipid metabolism genes in PCOS: a new insight into its pathogenesis. Clin. Epigenetics *10*, 6.
18. Xiao, H., Feng, X., Liu, M., Gong, H., and Zhou, X. (2023). SnoRNA and lncSNHG: Advances of nucleolar small RNA host gene transcripts in anti-tumor immunity. Front. Immunol. *14*, 1143980.
19. Williams, G.T., and Farzaneh, F. (2012). Are snoRNAs and snoRNA host genes new players in cancer? Nat. Rev. Cancer *12*, 84–88.
20. Biagioni, A., Tavakol, S., Ahmadirad, N., Zahmatkeshan, M., Magnelli, L., Mandegary, A., Samareh Fekri, H., Asadi, M.H., Mohammadinejad, R., and Ahn, K.S. (2021). Small nucleolar RNA host genes promoting epithelial-mesenchymal transition lead cancer progression and metastasis. IUBMB Life *73*, 825–842.
21. Li, Y.H., Hu, Y.Q., Wang, S.C., Li, Y., and Chen, D.M. (2020). LncRNA SNHG5: A new budding star in human cancers. Gene *749*, 144724.
22. Tay, Y., Rinn, J., and Pandolfi, P.P. (2014). The multilayered complexity of ceRNA crosstalk and competition. Nature *505*, 344–352.
23. Jinghua, H., Qinghua, Z., Chenchen, C., Lili, C., Xiao, X., Yunfei, W., Zhengzhe, A., Changxiu, L., and Hui, H. (2021). MicroRNA miR-92a-3p regulates breast cancer cell proliferation and metastasis via regulating B-cell translocation gene 2 (BTG2). Bioengineered *12*, 2033–2044.
24. Li, X., Wang, X., Cheng, Z., and Zhu, Q. (2020). AGO2 and its partners: a silencing complex, a chromatin modulator, and new features. Crit. Rev. Biochem. Mol. Biol. *55*, 33–53.
25. Creff, J., and Besson, A. (2020). Functional Versatility of the CDK Inhibitor p57(Kip2). Front. Cell Dev. Biol. *8*, 584590.
26. Stubbs, S.A., Stark, J., Dilworth, S.M., Franks, S., and Hardy, K. (2007). Abnormal preantral folliculogenesis in polycystic ovaries is associated with increased granulosa cell division. J. Clin. Endocrinol. Metab. *92*, 4418–4426.
27. Das, M., Djahanbakhch, O., Hacihanefioglu, B., Saridogan, E., Ikram, M., Ghali, L., Raveendran, M., and Storey, A. (2008). Granulosa cell survival and proliferation are altered in polycystic ovary syndrome. J. Clin. Endocrinol. Metab. *93*, 881–887.
28. Zhao, J., Xu, J., Wang, W., Zhao, H., Liu, H., Liu, X., Liu, J., Sun, Y., Dunaif, A., Du, Y., and Chen, Z.J. (2018). Long non-coding RNA LINC-01572:28 inhibits granulosa cell growth via a decrease in p27 (Kip1) degradation in patients with polycystic ovary syndrome. EBioMedicine *36*, 526–538.
29. Cataldo, N.A., Dumesic, D.A., Goldsmith, P.C., and Jaffe, R.B. (2000). Immunolocalization of Fas and Fas ligand in the ovaries of women with polycystic ovary syndrome: relationship to apoptosis. Hum. Reprod. *15*, 1889–1897.
30. Mikkelsen, A.L., Høst, E., and Lindenberg, S. (2001). Incidence of apoptosis in granulosa cells from immature human follicles. Reproduction (Cambridge, England) *122*, 481–486.
31. Mikaeili, S., Rashidi, B.H., Safa, M., Najafi, A., Sobhani, A., Asadi, E., and Abbasi, M. (2016). Altered FoxO3 expression and apoptosis in granulosa cells of women with polycystic ovary syndrome. Arch. Gynecol. Obstet. *294*, 185–192.
32. Ding, L., Gao, F., Zhang, M., Yan, W., Tang, R., Zhang, C., and Chen, Z.J. (2016). Higher PDCD4 expression is associated with obesity, insulin resistance, lipid metabolism disorders, and granulosa cell apoptosis in polycystic ovary syndrome. Fertil. Steril. *105*, 1330–1337.e3.
33. Raei Sadigh, A., Darabi, M., Salmassi, A., Hamdi, K., Farzadi, L., Ghasemzadeh, A., Fattahi, A., and Nouri, M. (2020). Fractalkine and apoptotic/anti-apoptotic markers in granulosa cells of women with polycystic ovarian syndrome. Mol. Biol. Rep. *47*, 3593–3603.
34. Lim, J.J., Han, C.Y., Lee, D.R., and Tsang, B.K. (2017). Ring finger protein 6 mediates androgen-induced granulosa cell proliferation and follicle growth via modulation of androgen receptor signaling. Endocrinology *158*, 993–1004.
35. Laird, M., Thomson, K., Fenwick, M., Mora, J., Franks, S., and Hardy, K. (2017). Androgen stimulates growth of mouse preantral follicles in vitro: interaction with follicle-stimulating hormone and with growth factors of the TGFβ superfamily. Endocrinology *158*, 920–935.
36. Billig, H., Furuta, I., and Hsueh, A.J. (1993). Estrogens inhibit and androgens enhance ovarian granulosa cell apoptosis. Endocrinology *133*, 2204–2212.
37. Tanaka, R., Satoh, H., Moriyama, M., Satoh, K., Morishita, Y., Yoshida, S., Watanabe, T., Nakamura, Y., and Mori, S. (2000). Intronic U50 small-nucleolar-RNA (snoRNA) host gene of no protein-coding potential is mapped at the chromosome breakpoint t(3;6)(q27;q15) of human B-cell lymphoma. Gene Cell. *5*, 277–287.
38. Qin, Y., Sun, W., Wang, Z., Dong, W., He, L., Zhang, T., Lv, C., and Zhang, H. (2022). RBM47/SNHG5/FOXO3 axis activates autophagy and inhibits cell proliferation in papillary thyroid carcinoma. Cell Death Dis. *13*, 270.
39. Damas, N.D., Marcatti, M., Côme, C., Christensen, L.L., Nielsen, M.M., Baumgartner, R., Gylling, H.M., Maglieri, G., Rundsten, C.F., Seemann, S.E., et al. (2016). SNHG5 promotes colorectal cancer cell survival by counteracting STAU1-mediated mRNA destabilization. Nat. Commun. *7*, 13875.
40. Kang, S., Ou, C., Yan, A., Zhu, K., Xue, R., Zhang, Y., and Lai, J. (2023). Long noncoding RNA SNHG5 induces the NF-κB pathway by regulating miR-181c-5p/CBX4 axis to promote the progression of non-small cell lung cancer. Arch. Bronconeumol. *59*, 10–18.
41. Ying, X., Zhang, W., Fang, M., Wang, C., Han, L., and Yang, C. (2020). LncRNA SNHG5 regulates SOX4 expression through competitive binding to miR-489-3p in acute myeloid leukemia. Inflamm. Res. *69*, 607–618.
42. Li, Y., Guo, D., Zhao, Y., Ren, M., Lu, G., Wang, Y., Zhang, J., Mi, C., He, S., and Lu, X. (2018). Long non-coding RNA SNHG5 promotes human hepatocellular carcinoma progression by regulating miR-26a-5p/GSK3β signal pathway. Cell Death Dis. *9*, 888.
43. Li, S., Shan, Y., Li, X., Zhang, C., Wei, S., Dai, S., Zhao, R., Zhao, X., Zhao, L., and Shan, B. (2019). lncRNA SNHG5 modulates endometrial cancer progression via the miR-25-3p/BTG2 axis. J. Oncol. *2019*, 7024675.
44. Lin, H., Shen, L., Lin, Q., Dong, C., Maswela, B., Illahi, G.S., and Wu, X. (2020). SNHG5 enhances Paclitaxel sensitivity of ovarian cancer cells through sponging miR-23a. Biomed. Pharmacother. *123*, 109711.
45. Han, Y., Huang, Y., Yang, Q., Jia, L., Zheng, Y., and Li, W. (2022). Long non-coding RNA SNHG5 mediates periodontal inflammation through the NF-κB signalling pathway. J. Clin. Periodontol. *49*, 1038–1051.
46. Liu, L., Chen, G., Chen, T., Shi, W., Hu, H., Song, K., Huang, R., Cai, H., and He, Y. (2020). si-SNHG5-FOXF2 inhibits TGF-β1-induced fibrosis in human primary endometrial stromal cells by the Wnt/β-catenin signalling pathway. Stem Cell Res. Ther. *11*, 479.
47. Zhao, Q., and Fan, C. (2019). A novel risk score system for assessment of ovarian cancer based on co-expression network analysis and expression level of five lncRNAs. BMC Med. Genet. *20*, 103.
48. Henique, C., Bollée, G., Loyer, X., Grahammer, F., Dhaun, N., Camus, M., Vernerey, J., Guyonnet, L., Gaillard, F., Lazareth, H., et al. (2017). Genetic and pharmacological inhibition of microRNA-92a maintains podocyte cell cycle quiescence and

limits crescentic glomerulonephritis. Nat. Commun. *8*, 1829.

49. Liu, J., Yao, W., Yao, Y., Du, X., Zhou, J., Ma, B., Liu, H., Li, Q., and Pan, Z. (2014). MiR-92a inhibits porcine ovarian granulosa cell apoptosis by targeting Smad7 gene. FEBS Lett. *588*, 4497–4503.
50. Lin, L., Du, T., Huang, J., Huang, L.L., and Yang, D.Z. (2015). Identification of differentially expressed microRNAs in the ovary of polycystic ovary syndrome with hyperandrogenism and insulin resistance. Chin. Med. J. *128*, 169–174.
51. Gupta, A., Vats, A., Ghosal, A., Mandal, K., Sarkar, R., Bhattacharya, I., Das, S., Pal, R., and Majumdar, S.S. (2022). Follicle-stimulating hormone-mediated decline in miR-92a-3p expression in pubertal mice Sertoli cells is crucial for germ cell differentiation and fertility. Cell. Mol. Life Sci. *79*, 136.
52. Fritz, I.B. (1982). Comparison of granulosa and sertoli cells at various stages of maturation: similarities and differences. Adv. Exp. Med. Biol. *147*, 357–384.
53. Hu, S., Liu, L., Chang, E.B., Wang, J.Y., and Raufman, J.P. (2015). Butyrate inhibits pro-proliferative miR-92a by diminishing c-Myc-induced miR-17-92a cluster transcription in human colon cancer cells. Mol. Cancer *14*, 180.
54. Stampone, E., Caldarelli, I., Zullo, A., Bencivenga, D., Mancini, F.P., Della Ragione, F., and Borriello, A. (2018). Genetic and epigenetic control of CDKN1C expression: importance in cell commitment and diffentiation, tissue homeostasis and human diseases. Int. J. Mol. Sci. *19*, 1055.
55. Jiang, Q., Miao, R., Wang, Y., Wang, W., Zhao, D., Niu, Y., Ding, Q., Li, Y., Leung, P.C.K., Wei, D., and Chen, Z.J. (2023). ANGPTL4 inhibits granulosa cell proliferation in polycystic ovary syndrome by EGFR/JAK1/STAT3-mediated induction of p21. FASEB J. *37*, e22693.
56. Takahashi, K., Nakayama, K., and Nakayama, K. (2000). Mice lacking a CDK inhibitor, p57Kip2, exhibit skeletal abnormalities and growth retardation. J. Biochem. *127*, 73–83.
57. Li, J.H., Liu, S., Zhou, H., Qu, L.H., and Yang, J.H. (2014). starBase v2.0: decoding miRNA-ceRNA, miRNA-ncRNA and protein-RNA interaction networks from large-scale CLIP-Seq data. Nucleic Acids Res. *42*, D92–D97.
58. Jeggari, A., Marks, D.S., and Larsson, E. (2012). miRcode: a map of putative microRNA target sites in the long non-coding transcriptome. Bioinformatics *28*, 2062–2063.
59. Rehmsmeier, M., Steffen, P., Hochsmann, M., and Giegerich, R. (2004). Fast and effective prediction of microRNA/target duplexes. RNA *10*, 1507–1517.
60. Owens, L.A., Kristensen, S.G., Lerner, A., Christopoulos, G., Lavery, S., Hanyaloglu, A.C., Hardy, K., Yding Andersen, C., and Franks, S. (2019). Gene expression in granulosa cells from small antral follicles from women with or without polycystic ovaries. J. Clin. Endocrinol. Metab. *104*, 6182–6192.
61. Byers, S.L., Wiles, M.V., Dunn, S.L., and Taft, R.A. (2012). Mouse estrous cycle identification tool and images. PLoS One *7*, e35538.
62. Caldwell, A.S.L., Edwards, M.C., Desai, R., Jimenez, M., Gilchrist, R.B., Handelsman, D.J., and Walters, K.A. (2017). Neuroendocrine androgen action is a key extraovarian mediator in the development of polycystic ovary syndrome. Proc. Natl. Acad. Sci. USA *114*, E3334–E3343.
63. Zhou, Y., Richard, S., Batchelor, N.J., Oorschot, D.E., Anderson, G.M., and Pankhurst, M.W. (2022). Anti-Müllerian hormone-mediated preantral follicle atresia is a key determinant of antral follicle count in mice. Hum. Reprod. *37*, 2635–2645.

STAR★METHODS

KEY RESOURCES TABLE

REAGENT or RESOURCE	SOURCE	IDENTIFIER
Antibodies		
Anti-FSHR	Proteintech Group	Cat# 22665-1-AP; RRID:AB_2631204
Anti-Bax	Cell Signaling Technology	Cat# 5023; RRID:AB_10557411
Anti-Bcl-2	Cell Signaling Technology	Cat# 15071; RRID:AB_2744528
Anti-β-actin	Cell Signaling Technology	Cat# 3700; RRID:AB_2242334
Anti-Ago2	Proteintech	Cat# 67934-1-Ig; RRID:AB_2918686
Anti-digoxin	Roche	Cat# 11207750910; RRID:AB_514501
Anti-p57	Abcam	Cat# ab75974; RRID:AB_1310535
Anti-mouse IgG, HRP-linked Antibody	Cell Signaling Technology	Cat# 7076; RRID:AB_330924
Anti-rabbit IgG, HRP-linked Antibody	Cell Signaling Technology	Cat# 7074; RRID:AB_2099233
Bacterial and virus strains		
H215 pAdeno-EF1a-MCS-MCMV-EGFP-3FLAG (AdNC)	Obio Technology (Shanghai)	N/A
pAdeno-EF1-SNHG5-MCMV-EGFP-3FLAG (AdSNHG5)	Obio Technology (Shanghai)	N/A
Biological samples		
Human granulosa cells	International Peace Maternity and Child Health Hospital	N/A
Critical commercial assays		
PrimeScript™ RT reagent kit with gDNA Eraser	Takara Bio	Cat# RR047Q
TB Green Premix Ex Taq	Takara Bio	Cat# RR420A
miRNA First Strand cDNA Synthesis (Tailing Reaction) kit	Sangon Biotech	Cat# B532451
Cell Counting Kit-8	Beyotime Biotech	Cat# C0038
EdU Cell Proliferation Kit	Beyotime Biotech	Cat# C0078S
FITC Annexin V Apoptosis Detection Kit I	BD Biosciences	Cat# 556547
Cell cycle kit	Absin	Cat# abs50005
PARIS kit	Thermo Fisher Scientific	Cat# AM1921
RNA-binding protein immunoprecipitation kit	Millipore	Cat# 17-700
Dual-Luciferase Reporter Assay System	Promega	Cat# E1910
Testosterone ELISA kit	R & D	Cat# KGE010
AMH ELISA kit	R & D	Cat# DY1737
Deposited data		
RNA-seq data	This paper	GEO: GSE246995
Experimental models: Cell lines		
KGN cell line	Procell	Cat# CL-0603
Experimental models: Organisms/strains		
Eight-week-old female C57BL/6 mice	SLAC ANIMAL	N/A
Oligonucleotides		
SNHG5 probe	TGCTAGTCAGTCACATTCGACA	QIAGEN
siRNAs and miRNAs, see Table S4	This paper	N/A
Primers, see Table S5	This paper	N/A

(*Continued on next page*)

Continued

REAGENT or RESOURCE	SOURCE	IDENTIFIER
Software and algorithms		
ImageJ	National Institutes of Health	https://imagej.net/ij/index.html
Starbase v2.0	Li et al.[57]	http://starbase.sysu.edu.cn/
miRcode	Jeggari et al.[58]	http://www.mircode.org/
RNAhybrid 2.2 software	Marc et al.[59]	https://bibiserv.cebitec.uni-bielefeld.de/rnahybrid/
BioRender	BioRender.com	https://www.biorender.com/about
R version 3.5.1	The R Foundation	https://www.r-project.org/
GraphPad Prism 8.0 Software	GraphPad Inc.	https://www.graphpad.com
SPSS 22.0 software	IBM SPSS	https://www.ibm.com/cn-zh/products/spss-statistics

RESOURCE AVAILABILITY

Lead contact

Further information and requests for resources and reagents should be directed to and will be fulfilled by the lead contact, Hefeng Huang (huanghefg@hotmail.com).

Materials availability

This study did not generate new unique reagents.

Data and code availability

The RNA-seq data have been deposited at Gene Expression Omnibus (GEO) and are publicly available as of the date of publication. Accession number is listed in the key resources table.

This article contains no original code.

Any additional information required to reanalyze the data reported in this paper is available from the lead contact upon request.

EXPERIMENTAL MODEL AND STUDY PARTICIPANT DETAILS

Human participants

Ovarian GCs were collected from Chinese women who received assisted reproduction technology treatment at the Reproduction Medicine Center, International Peace Maternity and Child Health Hospital, School of Medicine, Shanghai Jiao Tong University between January 2018 and December 2020. This study has been approved by the local Ethics Committee. All participants have provided written informed consent, and the study was performed in accordance with the Declaration of Helsinki. The diagnosis of PCOS was based on the Rotterdam Consensus for PCOS revised in 2003.[2] Women with infertility due to tubal or male factors served as controls. All control women had regular menstrual cycles, normal basal hormone levels, and normal ovaries on ultrasound. Demographic variables and endocrine characteristics of the subjects are presented in Tables S1, S2, and S3.

Primary cell cultures

Ovarian GCs were extracted from follicular fluid as previously described.[60] Briefly, follicular fluid was pooled and centrifuged at 2,000 rpm for 10 minutes. GCs were isolated by Ficoll-Paque density gradient centrifugation and washed with PBS. The isolated GCs were either frozen at -80°C for further analysis or digested using TrypLE (Gibco, Grand Island, New York, USA) and Accumax (Invitrogen, Carlsbad, CA, USA) for cell culture. GCs were cultured in Dulbecco's Modified Eagle Medium/Nutrient Mixture F-12 (DMEM/F12) (Gibco, Grand Island, New York, USA) containing 10% fetal bovine serum (FBS, Gibco, Grand Island, New York, USA) and 1% Antibiotic-Antimycotic (Gibco, Grand Island, New York, USA) and incubated at 37°C with 5% CO_2. Primary GCs were identified by detecting FSHR through immunofluorescence.

Cell lines

KGN cells were cultured under the same conditions and in the same medium as that of GCs, with the exception of the antibiotic used: penicillin-streptomycin (Gibco, Grand Island, New York, USA). KGN cells were subcultured when they reached about 80% confluency. KGN cells were identified by short tandem repeat PCR in May 2019, and no cross-contamination with other cells was observed.

Mice

Female C57BL/6 mice aged 8 weeks were used to establish the animal model and all mice were housed in a specific pathogen-free facility at Department of Laboratory Animal, School of Medicine, Shanghai Jiao Tong University. All experimental procedures were approved by the

Animal Care Committee in accordance with institutional animal care and use guidelines. Body weight was measured before surgery, and anesthesia was induced through intraperitoneal injection of 0.02 mL/g 1.25% tribromoethanol. The mice were subjected to the prone position, and a small transverse incision of about 1.0–2.0 cm was made at the middle-dorsal surface of the ovary. Derma, muscular layer, and peritoneum were cut to expose and extract the bilateral ovaries from the abdominal cavity. Recombinant adenovirus carrying lncRNA SNHG5 (AdSNHG5) or an empty adenovirus vector (AdNC) was injected into the bilateral ovaries based on the randomly assigned experimental group. Finally, the incision was stitched layer by layer and sprayed with antibiotics, and the mice were subjected to following experiments.

METHOD DETAILS

Cell transfection and treatment

KGN cells and GCs were seeded into six-well plates, cultured for 1 day, and then transfected with siRNAs (GenePharma, Shanghai, China), miRNA mimics (Sangon Biotech, Shanghai, China), or miRNA inhibitors (Sangon Biotech, Shanghai, China) using Lipofectamine 2000 reagent (Invitrogen, Carlsbad, CA, USA), according to the manufacturer's instructions. Sequences of the siRNAs, miRNA mimics and inhibitors are shown in Table S4.

Recombinant adenovirus carrying lncRNA SNHG5 (AdSNHG5, OBiO Technology, Shanghai, China) was constructed to overexpress SNHG5. Cells were inoculated with either AdSNHG5 or adenovirus vector (AdNC) at a multiplicity of infection (MOI) of 10.

After transfection or infection, the cells were incubated for a period ranging between 24-72 hours before further treatment.

RT-qPCR

The total RNA of cells and tissues was extracted using TRIzol (Invitrogen, Carlsbad, CA, USA), and cDNA was obtained using PrimeScript™ RT reagent kit with gDNA Eraser (Takara Bio, Tokyo, Japan). PCR primers (Table S5) were synthetized by BioSune Biotech (Shanghai, China) or Sangon Biotech, and the PCR was carried out as per the instructions of TB Green PCR kits (Takara Bio, Tokyo, Japan) on a QuantStudio 7 Flex Detection System (Applied Biosystems, CA, USA). GAPDH and U6 were used as internal references, as applicable. cDNA and RT-qPCR for miRNA were conducted using the miRNA First Strand cDNA Synthesis (Tailing Reaction) kit from Sangon Biotech, following the manufacturer's instructions. Data were analyzed using the 2-ΔΔCT method.

Western blot (WB)

Cells were harvested and lysed using radioimmunoprecipitation assay (RIPA) buffer (Thermo Fisher Scientific, USA) containing a protease and phosphatase inhibitor cocktail (Thermo Fisher Scientific, USA). Proteins were separated by SDS-PAGE, transferred onto polyvinylidene difluoride membranes, blocked with 5% skim milk, incubated with primary antibodies overnight at 4°C, and then incubated with horseradish peroxidase (HRP)–conjugated secondary antibodies. The blots were visualized using an enzyme chemiluminescence (ECL) reagent (Millipore, USA). β-Actin (Cell Signaling Technology, USA) was used as an internal reference for normalization. Details of the antibodies used in the WB analysis are listed in the key resources table.

Immunofluorescence (IF)

Cells were seeded onto chamber glass slides, fixed with 4% paraformaldehyde, blocked with blocking buffer containing 0.3% Triton X-100, incubated with the primary antibody overnight at 4°C, followed by incubation with the secondary antibody at room temperature for 1 hour. The slides were washed with phosphatebuffered saline (PBS) before mounting with DAPI (Abcam), and then visualized using a fluorescence microscope (Olympus, Tokyo, Japan). The antibodies used in IF are listed in the key resources table.

Cell proliferation assays

The relative cell viability was assessed using the Cell Counting Kit-8 (CCK-8, Beyotime Biotech, Shanghai, China) according to the manufacturer's instructions. Ethynyl-2-deoxyuridine (EdU) assays were conducted using the EdU Cell Proliferation Kit (Beyotime Biotech, Shanghai, China) in accordance with the manufacturer's protocols. The cells were observed using a fluorescence microscope to calculate the proportion of EdU-positive cells. All assays were replicated at least three times.

Flow cytometry

The percentage of cells undergoing apoptosis was quantified using the FITC Annexin V Apoptosis Detection Kit I (BD Biosciences) or APC Annexin V (BD Biosciences) along with 7-Amino-Actinomycin D (7-AAD, BD Biosciences) according to the manufacturer's protocols. Briefly, cells were collected, washed with PBS, incubated with Annexin V and a nucleic acid dye (either propidium iodide (PI) or 7-AAD) for 15 minutes at dark, and then analyzed by flow cytometry (FACSCalibur, Becton Dickinson, USA).

Cell cycle analysis was carried out using the Absin cell cycle kit (Absin, Shanghai, China) as per the instructions. Briefly, cells were harvested, fixed in 75% ethanol overnight at 4°C, and then incubated with RNaseA and PI for 30 minutes in the dark. Flow cytometry and ModFit LT software were employed to analyze the cells.

RNA-sequencing (RNA-seq)

Fourty-eight hours after transfection of either siRNA targeting SNHG5 or the control, KGN cells were harvested and RNA was extracted. After quality assessment, the RNA was sent for library preparation and RNA-seq by OEbiotech Co. (Shanghai, China). The RNA-seq data have been deposited at GEO, and accession number is provided in the key resources table. The differential expression mRNAs were identified by fold change (FC) and *p* value ($|\log2FC| \geq 1$ and p value < 0.05). Gene Set Enrichment Analysis (GSEA) was performed to interpret gene expression data.

Subcellular RNA fractionation analysis

Cytoplasmic and nuclear RNA were extracted using a PARIS kit (Thermo Fisher Scientific, USA) according to the manufacturer's instructions, followed by RT-qPCR assays. GAPDH and U6 were used as cytoplasmic and nuclear internal controls, respectively.

RNA-fluorescence *in situ* hybridization (FISH)

The SNHG5 probe, with the sequence TGCTAGTCAGTCACATTCGACA and digoxin labelled on both ends, was synthesized by QIAGEN (Germany). Cells were seeded onto chamber glass slides, fixed in 4% paraformaldehyde, digested with pepsin, and dehydrated using graded ethanol (70-100%). The slides were blocked by pre-hybridization buffer (Boster Biological Technology, Wuhan, China) for 2 hours at 54°C, followed by overnight hybridization with the SNHG5 probes in a humidified chamber at 54°C. After washing with a gradient SSC solution (Ambion), the slides were blocked with goat serum, incubated with rhodamine-conjugated anti-digoxin antibody (Roche) at 4°C overnight, washed with PBS, and mounted with DAPI (Abcam). The slides were visualized using a confocal laser scanning microscope (TCS SP8, Leica).

RNA immunoprecipitation (RIP)

RIP experiments were performed using an RNA-binding protein immunoprecipitation kit (Millipore, Bedford, MA, USA) according to the manufacturer's instructions. Cells were lysed in RIPA buffer containing a protease and phosphatase inhibitor cocktail, followed by incubation with magnetic beads conjugated with human anti-Ago2 antibody (Proteintech) or control normal mouse immunoglobulin G (IgG) in RIP buffer. After digestion with proteinase K and purification, the immunoprecipitated RNA was then extracted with Trizol and subjected to RT-qPCR analysis to detect the presence of the binding targets.

Dual-luciferase reporter assay

To determine the effect of miR-92a-3p on SNHG5, wildtype or mutant SNHG5 sequences were synthesized and cloned into the pGL3-basic firefly luciferase reporter (GeneCreat, China). To evaluate the effect of miR-92a-3p on the target gene, CDKN1C sequences containing wild-type or mutated binding sites for miR-92a-3p were synthesized and cloned into the pmirGLO luciferase vector. Luciferase activities were measured using the Dual-Luciferase Reporter Assay System (Promega) following the manufacturer's instructions.

Assessment of estrous cycle

The estrous cycle was monitored as previously described.[61] Briefly, vaginal swabs were collected at 8 am each day for 14 consecutive days. The swabs were smeared onto glass slides to air dry, stained with 0.5% toluidine blue, and then viewed under a light microscope. Estrous-cycle phase was determined based on the presence or absence of leukocytes, cornified epithelial, and nucleated epithelial cells.

Hormone assays

Mouse serum testosterone (T) and anti-Mullerian hormone (AMH) were determined using ELISA kits (R & D) according to the manufacturer's instructions. The mouse T detection limit was 0.03 ng/mL, with an intra-assay coefficient of variation (CV) of 3.3% and an inter-assay CV of 6.2%. The AMH ELISA kit had an assay range of 93.8–6000 pg/mL with unspecified intra-assay CV and interassay CV.

Ovary preparation and morphological analysis

Dissected ovaries were fixed in 4% paraformaldehyde and embedded in paraffin. Serial sections of 5 μm were stained with hematoxylin and eosin (H & E). Antral follicle count (AFC) and corpora lutea (CL) quantification were performed, sampling every 5th section of one ovary from each mouse according to previously reported methods.[62,63] Antral follicles include small antral follicles (oocyte surrounded by at least two layers of GCs and/or one or two small areas of small areas of FF) and large antral follicles (containing a large single antrum).

QUANTIFICATION AND STATISTICAL ANALYSIS

Data analyses were conducted using either SPSS 22.0 software (IBM SPSS, Chicago, IL, USA) or GraphPad Prism 8.0 Software (GraphPad Inc., San Diego, CA, USA). Student's t-test or Mann–Whitney test was used as appropriate for comparisons between groups, and one-way analysis of variance (ANOVA) or Kruskal-Wallis test with Bonferroni's correction was used for comparisons across multiple groups. Correlation analyses were performed using Spearman correlation test. $P < 0.05$ was considered statistically significant.